



Nanoscale

Effect of nanotube coupling on exciton transport in polymer-free monochiral semiconducting carbon nanotube networks

Journal:	<i>Nanoscale</i>
Manuscript ID	NR-ART-09-2019-007821.R1
Article Type:	Paper
Date Submitted by the Author:	19-Oct-2019
Complete List of Authors:	Arias, Dylan; National Renewable Energy Laboratory, Chemistry & Nanoscience Center Sulas-Kern, Dana; National Renewable Energy Laboratory, Hart, Stephanie; National Renewable Energy Laboratory, Chemistry and Nanoscience Center Kang, Hyun Suk; National Renewable Energy Laboratory, Hao, Ji; National Renewable Energy Laboratory, Chemistry & Nanoscience Center Ihly, Rachelle; NREL Johnson, Justin; NREL, Blackburn, Jeffrey; NREL, Ferguson, Andrew; National Renewable Energy Laboratory, Chemistry & Nanoscience Center

SCHOLARONE™
Manuscripts

Effect of nanotube coupling on exciton transport in polymer-free monochiral semiconducting carbon nanotube networks†

Dylan H. Arias,^a Dana B. Sulas-Kern,^b Stephanie M. Hart,^a Hyun Suk Kang,^a Ji Hao,^a Rachele Ihly,^a Justin C. Johnson,^a Jeffrey L. Blackburn^b and Andrew J. Ferguson^{*a}

Received 00th January 20xx,
Accepted 00th January 20xx

DOI: 10.1039/x0xx00000x

Semiconducting single-walled carbon nanotubes (s-SWCNTs) are attractive light-harvesting components for solar photoconversion schemes and architectures, and selective polymer extraction has emerged as a powerful route to obtain highly pure s-SWCNT samples for electronic applications. Here we demonstrate a novel method for producing electronically coupled thin films of near-monochiral s-SWCNTs without wrapping polymer. Detailed steady-state and transient optical studies on such samples provide new insights into the role of the wrapping polymer on controlling intra-bundle nanotube-nanotube interactions and exciton energy transfer within and between bundles. Complete removal of polymer from the networks results in rapid exciton trapping within nanotube bundles, limiting long-range exciton transport. The results suggest that intertube electronic coupling and associated exciton delocalization across multiple tubes can limit diffusive exciton transport. The complex relationship observed here between exciton delocalization, trapping, and long-range transport, helps to inform the design, preparation, and implementation of carbon nanotube networks as active elements for optical and electronic applications.

Introduction

Semiconducting single-walled carbon nanotubes (s-SWCNTs) have gained recent traction in the semiconductor community as a viable solution-processable material for thin film photovoltaics,¹⁻⁴ field effect transistors,⁵⁻⁷ digital logic circuits,⁸⁻¹¹ and thermoelectric devices.¹²⁻¹⁴ s-SWCNTs are appealing for these applications owing to their tunable optical, electronic, and mechanical properties. However, a key challenge in progress towards realizing high-performance devices is the isolation of desired s-SWCNTs from the polydisperse mixtures produced by most synthesis methods.¹⁵ Thus, suitable separation techniques allowing for isolation of desired semiconducting species that do not impede device efficiency will be required in the coming years for further development of SWCNT-based (opto-)electronic technologies.

Commercial techniques for generating SWCNTs from bulk carbon sources produce SWCNTs of varying diameters and chiralities.¹⁶ In most cases, approximately 1/3 of the raw SWCNTs have metallic band structure, while the remaining 2/3 are semiconducting with varying bandgaps according to their chiral structure.^{4, 14} Within the s-SWCNT population, further isolation based on optical/electrical band gap is typically desired for fundamental studies and device applications. While a

number of enrichment techniques have been demonstrated, one of the most popular relies on an appreciation of the complex van der Waals interactions between the pi-electron systems of the SWCNT and conjugated polymers,^{15, 17-20} that is capable of achieving >99.97% s-SWCNT purity^{21, 22} to enable digital electronic circuits based on carbon nanotube transistors.²³

Although this polymer sorting methodology allows for fast, inexpensive, and scalable separation of desired s-SWCNTs the technique has several drawbacks. The strong noncovalent polymer-nanotube binding typically leaves residual polymer in s-SWCNT thin films, potentially limiting charge^{12, 24-26} and/or exciton transport.²⁷⁻²⁹ Furthermore, leaving these conjugated polymers in the thin film instead of recycling them for future processing drives up the raw materials cost for this separation.²⁵ Strategies to remove these conjugated polymers from SWCNT networks include modifications to the polymer conformation,^{30, 31} as well as depolymerization via dissociation of covalent,^{32, 33} coordination,³⁴ or hydrogen bonds.^{26, 35, 36}

The supramolecular polymer-based separation strategy utilizes monomers that can self-assemble in solution through inter-monomer interactions, such as hydrogen bonding.^{26, 35, 36} These strategies may be particularly useful for future commercial applications, since the monomer units can be recycled following removal from the SWCNT networks to reduce processing costs.²⁵ The removal of these supramolecular polymers in the solid state, after s-SWCNT network deposition, has been shown to significantly improve charge carrier transport within the network.^{12, 24-26} While this supramolecular polymer dispersion strategy has been utilized to produce polymer-free s-SWCNT networks containing broad distributions

^a Chemistry & Nanoscience Center, National Renewable Energy Laboratory, Golden, Colorado 80401, United States. Email: andrew.ferguson@nrel.gov

^b Materials Science Center, National Renewable Energy Laboratory, Golden, Colorado 80401, United States.

† Electronic Supplementary Information (ESI) available: Materials and Methods. See DOI: 10.1039/x0xx00000x

of s-SWCNT diameters and band gaps, it has not been applied to near-monochiral s-SWCNT samples desired for fundamental studies of charge and/or exciton transport, or applications such as thin-film photovoltaics and photodetectors.

In this work, we overcome the diameter/chirality independent s-SWCNT selectivity of the 1,1'-(((1*E*,1'*E*)-(9,9-didodecyl-9*H*-fluorene-2,7-diyl)bis(ethene-2,1-diyl))bis(6-methyl-4-oxo-1,4-dihydropyrimidine-5,2-diyl))bis(3-dodecylurea) supramolecular polymer (SMP)^{12, 26} by demonstrating a simple polymer exchange process. The exchange process relies upon replacing highly-selective, long-chain fluorene-based polymers that yield near-monochiral (6,5) or (7,5) s-SWCNT samples with the removable SMP that subsequently enables the fabrication of polymer-free electronically coupled near-monochiral networks. We show that the samples wrapped in SMP exhibit subtle shifts in the s-SWCNT excitonic transitions relative to those wrapped by the bound fluorene-based polymers, which we attribute to changes in the polymer-induced strain on the nanotube lattice. Transient absorption (TA) spectroscopic measurements suggest more rapid downhill exciton energy transfer within polymer-free bundles, as well as a higher degree of exciton delocalization over majority species. The delocalization appears to hinder diffusive exciton transport between larger bandgap majority species, whereas rapid downhill energy transfer can 'trap' excitons energetically in small bandgap minority species, which are nevertheless capable of long-range diffusive transport.

Results and discussion

The SWCNT species present in raw soot of commercial CoMoCAT material (Signis SG65i; CHASM Advanced Materials Inc.) are illustrated in Fig. 1a and chemical structures of the selective wrapping polymers are shown in Fig. 1b. The SMP chemical structure shows a single monomer unit—the polymer is formed by hydrogen-bonding, self-association between terminal 2-ureido-6[1*H*]-pyrimidinone moieties on neighbouring monomers. SMP appears to disperse s-SWCNTs universally,^{24, 26} irrespective of diameter or chirality, resulting in ca. 10 unique SWCNT species identified in SMP CoMoCat dispersions, shown by the first excitonic transitions, S_{11} , in Fig. 1c. To overcome this limitation, we developed a polymer exchange process, where the highly-selective fluorene-based polymers, 9,9-dioctylfluorenyl-2,7-diyl (PFO) or PFO-BPy, are replaced by SMP in a dynamic binding exchange process driven by the presence of excess SMP in a tip-sonicated mixture.

The polymer exchange process involves preparing an initial dispersion of near-monochiral (6,5) or (7,5) s-SWCNTs by tip sonicating the SG65i raw material in a solution of PFO-BPy or PFO, respectively. An immediate short centrifuge step precipitates metallic SWCNTs, bundles, and other impurities into a 'pellet' from which the enriched s-SWCNT dispersion can be easily removed. Excess PFO-BPy/PFO is subsequently removed by an overnight (12 – 20 hours) ultracentrifuge step, followed by tip sonication of the resulting PFO-BPy:(6,5) or PFO:(7,5) pellet with excess SMP (1 mg/mL in toluene). A second overnight (12 – 20 hours) ultracentrifuge step is employed to

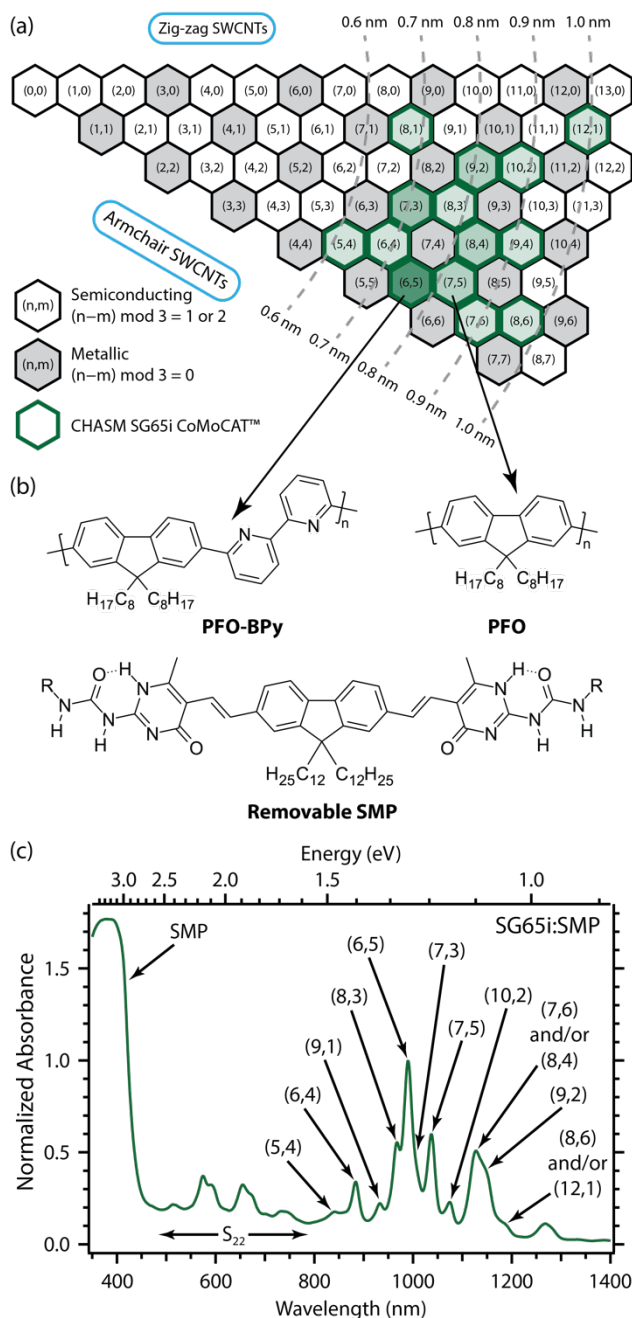


Fig. 1 (a) Graphene lattice 'chiral map' illustrating the chiral s-SWCNT species identified in the Technical Data Sheet for CHASM Signis SG65i (green hexagons). (b) Chemical structures of the fluorene-based polymers used for selective extraction of s-SWCNTs species from the CHASM Signis SG65i raw material. (c) Absorption spectrum, normalized to the peak for the (6,5) s-SWCNT, for a dispersion of SG65i using SMP—the S_{11} excitonic transitions for the chiral s-SWCNT species in the dispersion are identified, along with the region for the S_{22} excitonic transitions, and the SMP absorption.

remove unbound SMP and the exchanged/unbound PFO-BPy/PFO, leaving behind a pellet of SMP:(6,5) or SMP:(7,5) that can be readily re-dispersed into toluene, to form an ink for spectroscopic characterization or network deposition.

The general process of polymer exchange has been demonstrated for different SWCNT wrapping polymers,^{33, 37} including replacement of a selective bound polymer by an unselective cleavable polymer for multi-chiral SWCNT samples.³³ However, our specific development of polymer

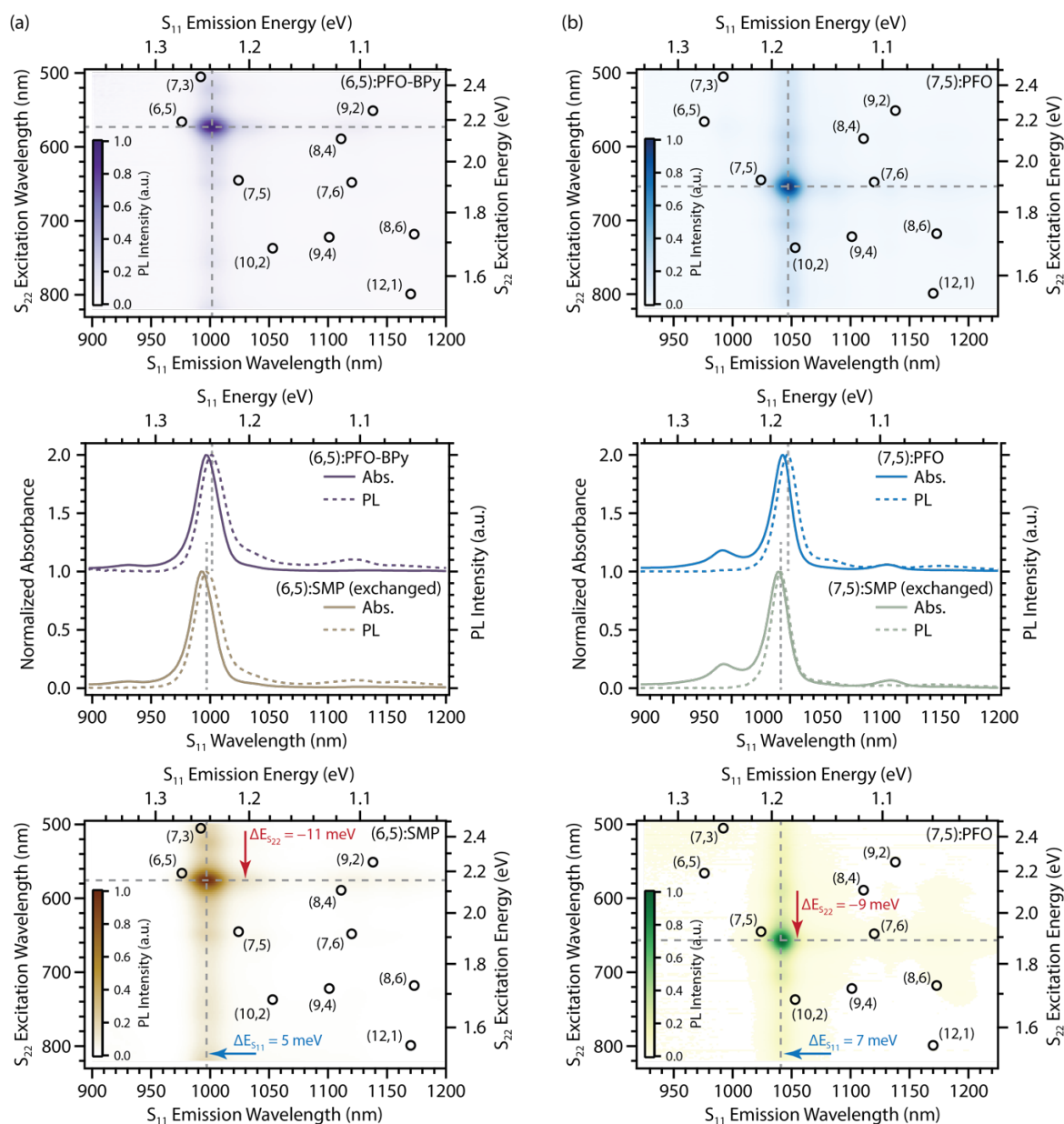


Fig. 2 Solution-phase photoluminescence excitation contour maps illustrating the effect of polymer exchange from the selective fluorene-based polymer (top) to the supramolecular polymer (bottom) on the excitonic transitions for (a) PFO-BPy-wrapped (6,5)-s-SWCNTs and (b) PFO-wrapped (7,5)-s-SWCNTs. The arrows indicate the direction and magnitude of the shift of the photoluminescence excitation peak for the SMP sample relative to the selective fluorene-based polymer; blue = hypsochromic shift and red = bathochromic shift. The middle panels show the normalized absorbance and photoluminescence spectra at the S_{11} region of the dominant s-SWCNT chirality.

exchange using a universally-selective and cleavable polymer has important and novel implications. The ability of SMP to universally disperse semiconducting SWCNTs, regardless of their diameter, may enable preparation of other polymer-free monochiral samples via replacement of any wrapping polymer selective for a single chirality and subsequently undergoing complete cleavage and removal of the SMP. We further note that material recycling of both the wrapping polymer and cleaved SMP remains facile, as the large difference in their molecular weights is well suited for separation via preparative chromatography. The SMP exchange method thus opens avenues for creating a wide range of high-quality monochiral SWCNT networks where strong electronic coupling is desired.

Isolation of individualized near-monochiral s-SWCNTs was confirmed by observation of a single, dominant cross-peak in the solution-phase photoluminescence excitation (PLE) contour maps (top and bottom panels in Fig. 2) and a single, dominant peak in the absorbance and photoluminescence spectra in the S_{11} region (middle panels of Fig. 2). In the sample dominated by the (6,5) species, the primary minority species is the (7,5) species, contributing about 5% to the measured absorbance spectrum. For the (7,5)-rich sample, there appears to be contributions to the absorbance spectrum of ca. 17% and ca. 5% due to minority (6,5) and (7,6) species, respectively.

The arrows in the bottom panels of Fig. 2 indicate that substitution of PFO-BPy/PFO for SMP results in a hypsochromic shift of the S_{11} and a bathochromic shift of the S_{22} excitonic

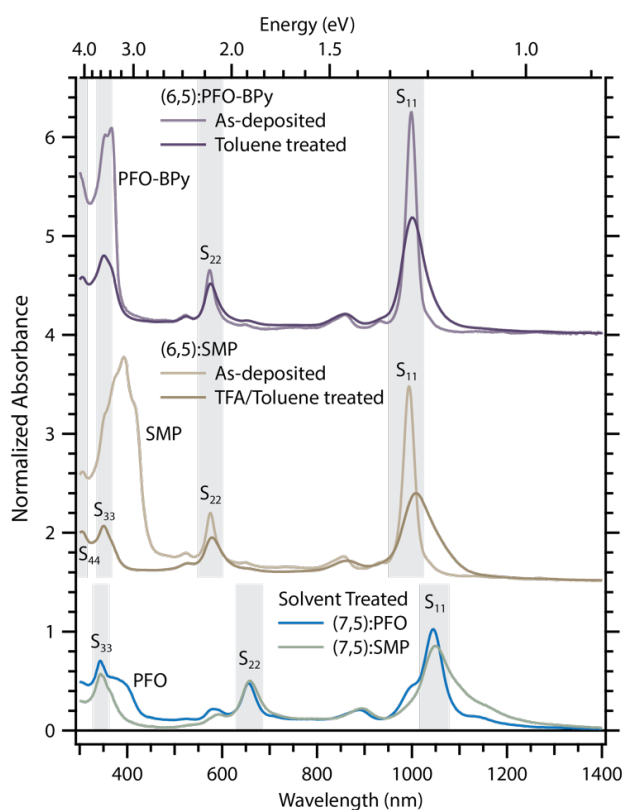


Fig. 3 Absorbance spectra for (6,5) and (7,5) s-SWCNT networks. Spectra illustrating the effect of the polymer removal solvent treatment for the (6,5):PFO-BPy (purple traces; top) and (6,5):SMP (brown traces; middle) samples. The lower traces show the spectra for solvent treated (7,5):PFO (blue trace) and (7,5):SMP (green trace) samples. The grey bands indicate the position of the s-SWCNT excitonic transitions.

transitions. Since the first two excitonic transitions move in opposite directions, we rule out solvatochromic or dielectric effects, which would be expected to shift both transitions in the same direction, as is observed for SWCNTs dispersed by polymers in organic solvents relative to aqueous dispersions.^{38–40} Instead, we attribute the shifts to changes in strain induced by the different wrapping polymers,^{41–43} which are discussed in more detail in the supplementary information.

Thin film networks of randomly oriented SWCNTs were prepared for spectroscopic studies by an ultrasonic spray deposition technique described previously.^{3, 12, 44} Absorption spectra shown in Fig. 3 illustrate that the excess polymer in (6,5):polymer networks prevents significant electronic interactions between individual SWCNTs, maintaining reasonably narrow excitonic optical transitions. Subsequent removal of excess polymer (PFO-BPy) or quantitative polymer removal (SMP) results in broadening and red-shift of the excitonic transitions (particularly the S_{11}). These observations point toward the formation of bundles that are dominated by strong electronic coupling between individual SWCNTs, with an additional contribution from inhomogeneous broadening due to environmental fluctuations (vide infra). Figure 3 indicates that the strength of the electronic coupling, as determined by the magnitude of the bathochromic shift and broadening of the S_{11} excitonic transition, is larger in solvent-treated SMP networks, as expected for quantitative removal of insulating polymer from the SWCNT surface.

The large aspect ratio of SWCNTs, coupled to their highly delocalized electronic structure, suggests that networks of s-SWCNTs could facilitate efficient exciton transport, provided a good understanding can be developed of the factors affecting the electronic coupling in and between nanotube bundles. Early work on the partial replacement of a single-strand DNA sequence with an anionic surfactant on the surface of the s-SWCNTs illustrated that bundle formation can give rise to efficient downhill exciton energy transfer to low bandgap (large diameter) chiral species within individual bundles.⁴⁵ A number of subsequent studies, employing transient absorption and time-resolved luminescence measurements of polymer-wrapped, small-diameter, multi-chiral s-SWCNT samples, have demonstrated ultrafast downhill exciton energy transfer (on timescales less than 10 ps) to the large-diameter nanotubes within the chiral distribution.^{27, 46} The rate and efficiency of the exciton energy transfer process can be manipulated by: (i) isolation of individualized s-SWCNTs into a polymer matrix,²⁷ (ii) deposition or processing conditions that influence network morphology,⁴⁷ and (iii) formation of networks where the wrapping polymer content is reduced.⁴⁸ Mehlenbacher et al. employed an ultrafast two-dimensional white light spectroscopy technique to demonstrate complex energy transfer pathways, particularly in the higher exciton manifolds, in networks of polymer-wrapped multi-chiral s-SWCNTs.⁴⁹ The formation of bare s-SWCNT networks, deposited from dispersions prepared via the aqueous two-phase (ATP) separation technique, results in strong inter-tube electronic coupling that manifests sub-ps intra- and inter-bundle energy transport.²⁸

In contrast to these previous studies, the approach we describe above allows for the preparation of both polymer-wrapped and polymer-free near-monochiral samples of various majority species that experience identical processing conditions (i.e., entirely in organic solvents). Additionally, we employ a combination of spectrottemporal transient absorption (TA) and TA anisotropy measurements, that allow us to decouple energetic effects from long-range exciton migration. Before discussing the observed transient spectroscopic signatures in more detail, we briefly consider a framework for the energy transfer and migration pathways available to excitonic excited states in the coupled s-SWCNT networks (Fig. 4). Strong inter-

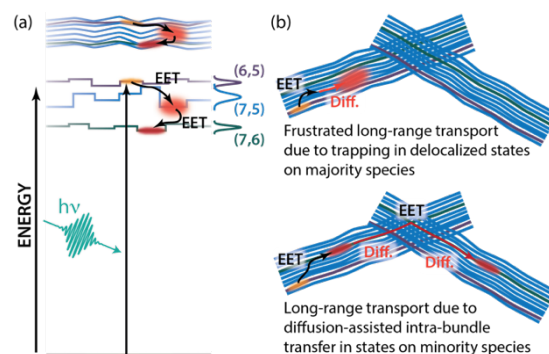


Fig. 4 Schematic illustrating (a) downhill electronic energy transfer (EET) in the excited state manifold associated with the various chiral s-SWCNT species within a bundle and (b) the impact of the downhill EET on exciton migration due to intra-bundle diffusion (Diff.) and inter-bundle EET at bundle-bundle junctions.

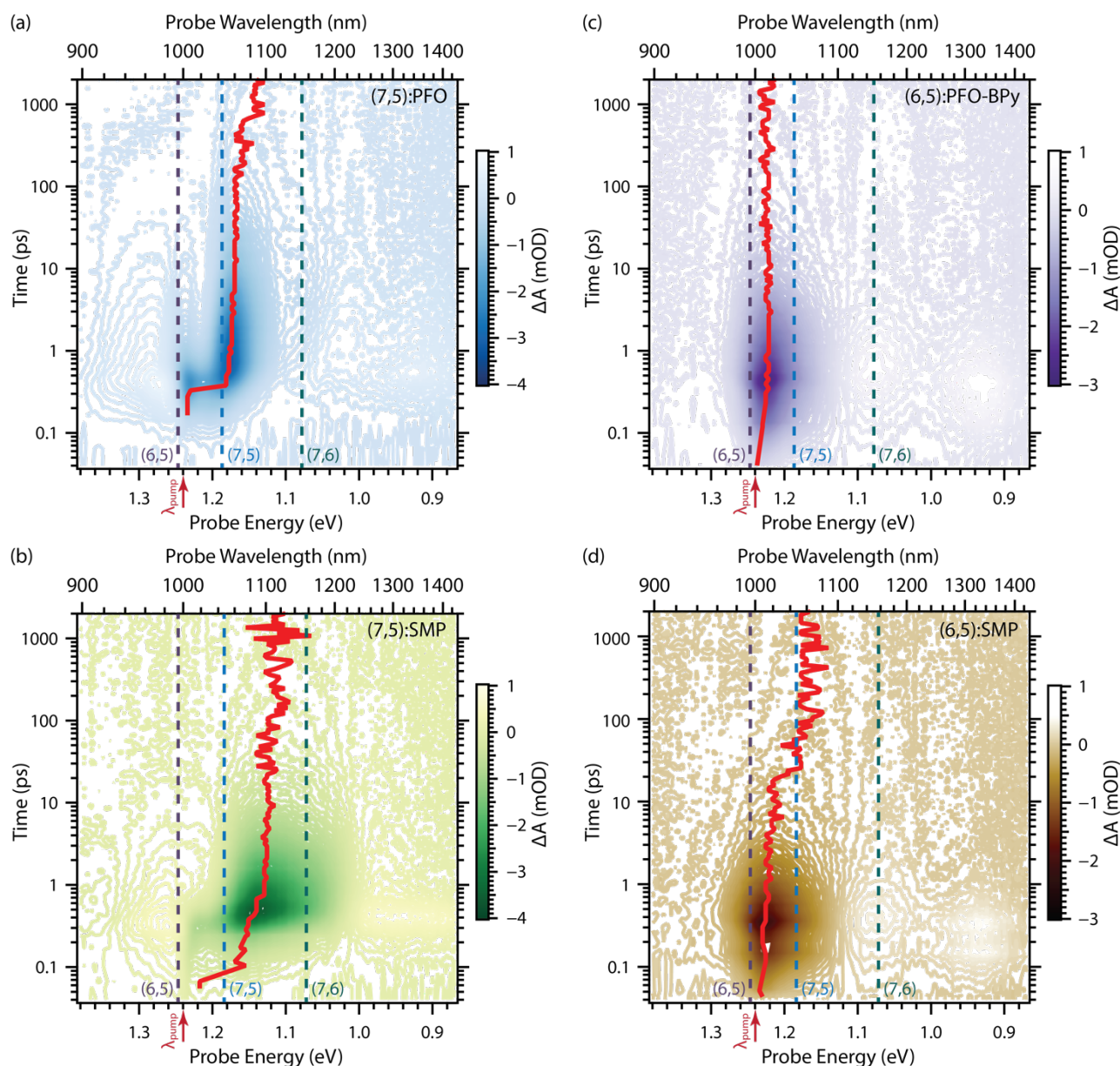


Fig. 5 Transient absorption spectra in the region of the S_{11} excitonic transitions illustrating the time-dependent downhill energy migration in (7,5) and (6,5) enriched s-SWCNT networks. 2D transient absorption maps for (a) (7,5):PFO and (b) (7,5):SMP networks and (c) (6,5):PFO-BPy and (d) (6,5):SMP networks. The red traces indicate the time-dependent peak energy of the transient spectrum. The dashed lines indicate the energetic positions of the S_{11} excitonic transitions for the different chiral species expected in each sample, determined from the ground state absorption (GSA) spectra, shown in Figs. S5 and S6 for comparison. The red arrows indicate the pump wavelength.

tube electronic coupling (particularly between neighboring majority species) results in instantaneous delocalization of the excited state wavefunction over multiple nanotubes within a bundle (c.f., the broadened and red-shifted absorption spectra). Excitons located in the excited-state manifold associated with majority species in a bundle can undergo ultrafast, time-dependent downhill energy transfer to either the lowest bandgap states in that inhomogeneously broadened manifold and/or to low bandgap, minority 'trap' species. These processes result in excited state population that resides in delocalized states of majority species or in localized minority states within a bundle. To this point we have only considered energetic effects, and the states described above can be considered energetic 'traps' that alter the population of excited states capable of long-range energy migration. The photoinduced

excited states, including those that are energetically 'trapped', can also undergo intra-bundle exciton diffusion to the junctions between bundles. Depending on the strength of the electronic coupling between energy donor and acceptor components across the junction, they may subsequently undergo inter-bundle energy transfer at the junction.

Figure 5 illustrates the impact of polymer removal on the transient photophysics of near-monochiral s-SWCNT networks, where stronger coupling in SMP-treated samples results in an accelerated exciton energy cascade to the lowest-energy minority s-SWCNT species. We rationalize the slower kinetics in samples containing residual polymer by considering that this residual polymer would be expected to frustrate downhill exciton energy transfer.²⁷⁻²⁹

Figure 5a shows TA spectra for the (7,5):PFO sample excited at the largest bandgap (6,5) minority species at 1,000 nm. The red line highlights the continuous bathochromic shift of the ground state bleach (GSB) over 2 ns, which we attribute to the downhill exciton energy cascade. Initially, the TA spectrum is dominated by GSB features associated with both the (6,5) and (7,5) species. Using global target analysis (Fig. 6c), we separate the individual *s*-SWCNT components and determine that the (7,5) GSB continues to rise for ca. 100 fs after the (6,5) has reached a maximum value. We attribute this additional rise time for the (7,5) species to exciton transfer from the (6,5) SWCNTs. The (6,5) species then decays with multiexponential kinetics corresponding to an amplitude-averaged lifetime of ca. 4 ps with 70% of the amplitude dominated by the initial 0.3 ps decay component.

After the GSB associated with the (7,5) majority species reaches a maximum value, we observe a time-dependent bathochromic shift, suggesting downhill energy migration to an S_{11} (7,5) excited state delocalized over multiple *s*-SWCNTs that are electronically coupled within a bundle or within an inhomogeneous distribution of exciton states. The (7,5) species does not fully decay within the 5 ns time window, and it exhibits multiexponential decay dominated by 3.1 ps and 60 ps time constants representing 71% and 26% of the GSB amplitude, respectively. The GSB associated with the (7,6) minority species grows in with a rise time of 1.2 ps (see Fig. 6c), suggesting fairly slow downhill exciton energy transfer to this minority species. We note that the 1.2 ps rise time for the (7,6) species is faster than either of the dominant decay components that we extract for the (7,5) majority species, suggesting that some direct energy transfer to the (7,6) from the (6,5) SWCNTs may also take place on faster time scales. At later times, the fractional amplitude of the remaining transient bleaching continues to shift toward the (7,6) species, though GSB for both (7,5) and (7,6) species remain at the end of our 5 ns window.

TA data for the (7,5):SMP films (Fig. 5b) exhibit broadly similar behaviour, except that the energy transfer kinetics are greatly accelerated. Even at very early times (<250 fs), the GSB for the (7,5) majority species dominates the TA spectrum, and there is already significant spectral contribution from the (7,6) minority species. Our global target analysis in Fig. 6d shows that all three species rise with the instrument response, and the (6,5) species fully decays over the following 0.6 ps. This result indicates extremely efficient exciton energy transfer from (6,5) SWCNTs to the (7,5) majority species. The bathochromic shift of the (7,5) species also takes place over only 0.6 ps, which is almost 100 times faster than in the (7,5):PFO films. This accelerated bathochromic shift in the polymer-free sample, in addition to the larger magnitude of the (7,5) GSB bathochromic shift compared to the PFO case, is consistent with the expectation that polymer removal results in a greater fraction of strongly coupled (7,5) nanotubes that enable more rapid and efficient downhill energy transfer in the excited-state manifold of the majority SWCNTs.

Figures 5c,d and 6a,b show that samples enriched in (6,5) *s*-SWCNTs exhibit qualitatively similar dynamics to the (7,5) *s*-SWCNT networks. In (6,5):PFO-BPy films, the TA spectrum is

dominated by the (6,5) GSB for the entire decay, indicating that downhill energy transfer to the (7,5) minority species is inhibited by the PFO-BPy wrapping polymer. The (6,5) GSB in (6,5):PFO-BPy films exhibits multiexponential decay with a 230 ps amplitude-averaged time constant. In contrast, the (6,5):SMP sample shows accelerated decay of the (6,5) species with an average time constant of 3.6 ps, where the initial 0.9 ps decay component (representing 87% of the (6,5) GSB amplitude) is concomitant with the rise of a lower-energy species. We assign this lower-energy species in the SMP-treated samples primarily to the (7,5) minority species, though the GSB peak broadening suggests that the bathochromic shift of the (6,5) species may also contribute to the long-delay spectra. Taken together, these results further support that removal of the wrapping polymer allows for downhill energy migration to minority species and delocalized states that are more strongly coupled in the absence of any wrapping polymer.

In addition to the accelerated exciton cascade to low-energy minority species in the SMP-treated samples, we note that the overall decay to the ground state appears to be faster upon polymer removal. The faster exciton decay observed for the SMP samples could be attributed to the following: (1) reduced lifetime due more efficient funnelling of excitons to smaller bandgap minority species (i.e., energy gap law for excited state decay), (2) enhanced higher-order (i.e., Auger) recombination due to a local increase in the exciton concentration caused by confinement to low bandgap nanotubes, or (3) improved intra-bundle transport that facilitates exciton recombination or trapping at defects.

Although the TA data in Fig. 5 provide compelling evidence for rapid downhill exciton energy transfer, both to low-energy minority species and delocalized states, these data cannot provide information regarding the spatial nature of long-range exciton transport in these near-monochiral networks. In other words, it is unclear whether downhill energy transfer occurs primarily within a SWCNT bundle, between different SWCNT bundles, or both. For this, we turn to the TA anisotropy technique originally employed to probe exciton transport in similar enriched *s*-SWCNT networks.^{27,47}

Figure 6 (bottom panels) presents the time-dependent transient absorption anisotropy, $r(t)$, following linearly polarized excitation of *s*-SWCNT networks prepared either with residual polymer (PFO-BPy or PFO) or with the removable SMP. We report the transient anisotropy as

$$r(t) = \frac{TA_{\parallel} - TA_{\perp}}{TA_{\parallel} + TA_{\perp}} \quad (1)$$

where TA_{\parallel} is the signal for pump and probe pulses with parallel polarization and TA_{\perp} is the signal for cross-polarized pump and probe pulses. The initial anisotropy value is expected to be 0.5 for linearly-polarized excitation of a planar array of isotropically-oriented 1D dipoles, which is a reasonable representation of thin-film networks containing large aspect ratio *s*-SWCNTs. Any decrease in anisotropy over time indicates exciton energy transfer to SWCNTs with different alignment. Loss of anisotropy can thus be interpreted as energy transfer between un-aligned bundles, while retention of anisotropy

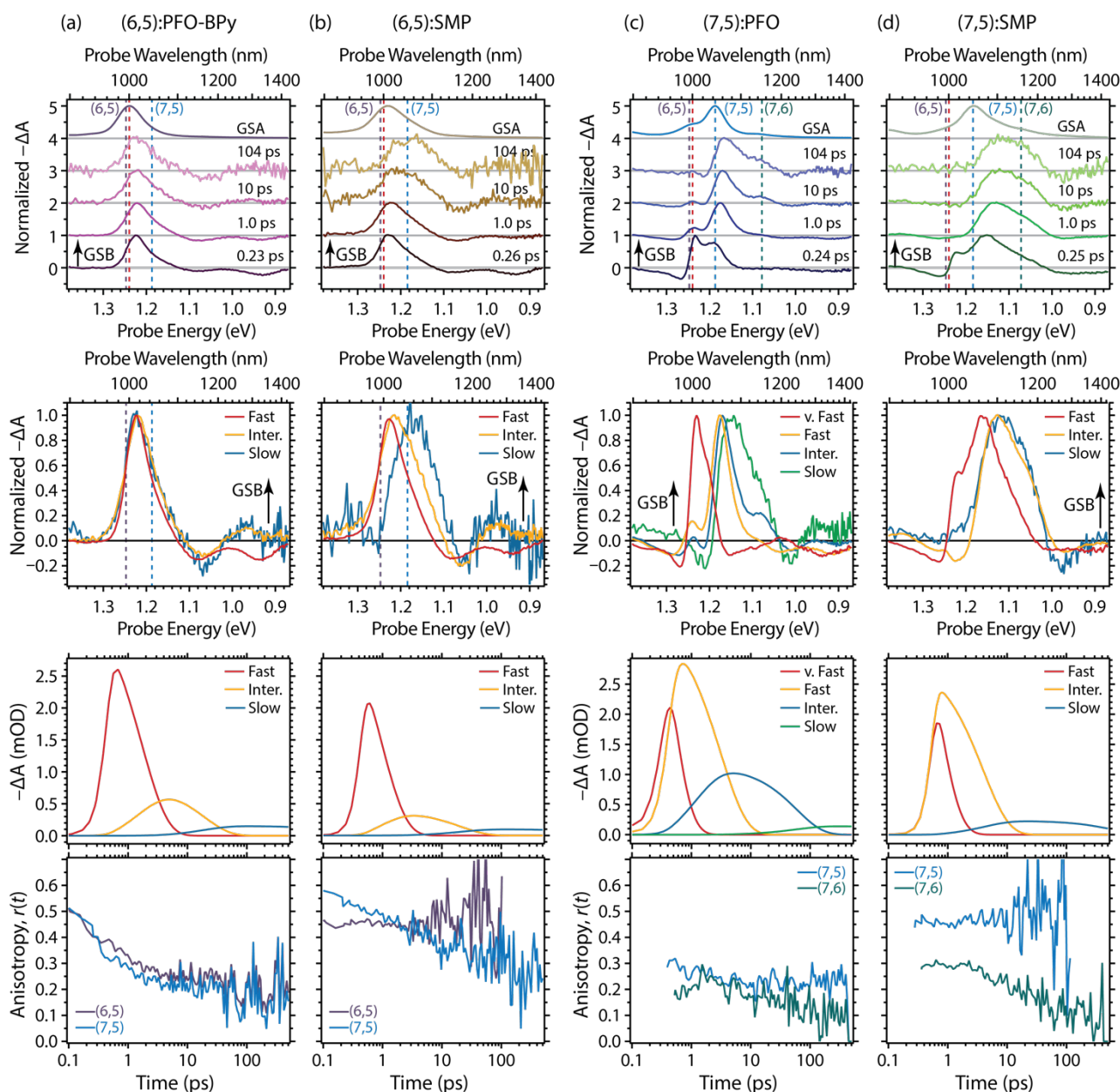


Fig. 6 Summary of the transient absorption data for the (a) (6,5):PFO-BPy, (b) (6,5):SMP, (c) (7,5):PFO, and (d) (7,5):SMP s-SWCNT networks. Normalized time-dependent absorption spectra (top row); Spectral components (second row) and associated kinetic traces (third row) extracted from global target analysis of the 2D TAS maps shown in Fig. 4; and Transient absorption anisotropy (bottom row).

(when paired with observation of downhill energy transfer in the standard TA measurement) suggests transfer between aligned nanotubes within s-SWCNT bundles.

For both (6,5)-enriched samples pumped and probed at 1000 nm (Fig. 6a,b; bottom panels), at the S_{11} transition of the (6,5) majority species, the anisotropy begins at roughly 0.5, as expected for the randomly oriented SWCNTs. The subsequent evolution of $r(t)$ for the (6,5):PFO-BPy sample is rapid, decreasing to 0.25 within about 5 ps, suggesting that energy transfer between (6,5) species occurs between nanotubes with different orientation, randomizing the distribution of exciton dipoles. The signal then plateaus for the remaining delay time window. When probed at 1050 nm, the position of the (7,5) S_{11} GSB, the anisotropy decay for the (6,5):PFO-BPy sample matches that for the 1000 nm probe, suggesting that excitations

residing on minority (7,5) species are also able to transfer to (7,5) SWCNTs with different orientations.

In contrast, for the (6,5):SMP sample (Fig. 6b; bottom panel), the value of $r(t)$ at the (6,5) S_{11} GSB remains constant, suggesting that excitations are trapped on the same (6,5) nanotubes/bundles in the absence of wrapping polymer. We note that the noise becomes large, especially beyond 5 ps, in the SMP sample due to the rapid decay of the (6,5) S_{11} GSB. Interestingly, the TA anisotropy for the (7,5) minority species at 1050 nm shows a different anisotropy decay compared to the (6,5) majority species, with the (7,5) probe exhibiting a steady decrease in $r(t)$ over the entire time delay. This suggests that polymer removal does not hinder energy transfer between minority (7,5) species with different alignment.

The (7,5) samples were also pumped at 1000 nm, representing excitation of minority (6,5) species, and probed at 1050 nm (Fig. 6c,d; bottom panels). Much like for the (6,5):SMP sample, the anisotropy for the majority (7,5) species in the (7,5):SMP sample begins at roughly 0.5 and shows no discernible decay through 25 ps. However, the anisotropy decays steadily in the (7,5):SMP sample when probed at the S_{11} GSB of the minority (7,6) species at 1150 nm. This result suggests that in the strongly-coupled polymer-free films, excitons in majority species are not able to undergo appreciable diffusion-assisted inter-bundle transfer, whereas this process remains viable for the minority species in both types of samples.

The majority (7,5) species in the (7,5):PFO sample, probed at 1050 nm, exhibits an initial anisotropy around 0.3 that then decays to roughly 0.25 in a few ps, where it remains for the delay time window. The wavelength dependence for the (7,5):PFO sample mirrors that observed for the polymer-wrapped (6,5) samples, with $r(t)$ unchanged regardless of whether the probe wavelength is set to the majority (7,5) species or minority (7,6) species. This result is consistent with active inter-bundle energy transfer for both samples where the wrapping polymer has not been removed. The work of Grechko et al.⁴⁷ suggests that this anisotropy decay can be assigned to diffusion-limited inter-bundle exciton transport.

We assign the differences in anisotropy between (6,5):SMP and (6,5):PFO-BPy samples to enhanced downhill energy transfer in the absence of wrapping polymer, which appears to outcompete ultrafast inter-bundle energy transfer. As shown in the TA (Fig. 5), strong inter-tube coupling leads to fast sub-ps downhill energy transfer in (6,5):SMP samples that is largely absent in (6,5):PFO-BPy samples. Therefore, rapid discovery of low energy "trap" sites inhibits energy transfer between bundles of isoenergetic (6,5):SMP SWCNTs, which would otherwise lead to anisotropy decay. For (6,5):PFO-BPy films that lack ultrafast trapping, the first roughly 5 ps after photoexcitation is dominated by inter-bundle energy transfer, leading to decay in $r(t)$. The discovery of "trap" sites may still occur in these samples but at a slower rate, and this eventually arrests the inter-bundle transfer on timescales longer than 5 ps and leads to the plateau in $r(t)$. Although the microscopic rate constants are unknown, we hypothesize that the ratio of the rates of trapping in low energy tubes vs. inter-bundle energy transfer will be proportional to the anisotropy values observed at longer delay times.

The wavelength dependence observed for the (6,5):SMP samples may reveal further information about the nature of traps. We envision that traps in a majority (6,5) sample will be larger diameter nanotube impurities (e.g., (7,5)) or delocalized states with lower energy resulting from strong interactions between (6,5) tubes. In addition, the latter states may inhibit fast inter-bundle exciton migration because they may lack the combination of favorable spectral overlap and transition dipole coupling that hastens energy transfer for localized excitations.⁵⁰ Evidence for these delocalized states is found in the broadened and shifted TA features of SMP samples. On the other hand, if energy transfer to (7,5) impurities dominates over transfer to delocalized states, then the energetic and spatial isolation may

inhibit further delocalization over (6,5) majority aggregates. Localization on the (7,5) impurities may thus enable inter-bundle energy transfer to other (7,5) tubes. This picture is consistent with the enhanced decay in $r(t)$ when minority (7,5) tubes are probed.

For the (7,5)-majority samples, the anisotropy trends are largely the same as in the (6,5) films. However, the lower initial value of $r(t)$ for the (7,5):PFO sample is notable and suggests a more rapid inter-bundle energy transfer process (i.e., within the roughly 200 fs instrument response) compared to the (6,5):PFO-BPy sample. This observation may be related to efficient inter-bundle energy transfer facilitated by rapid downhill energy transfer from the photoexcited minority (6,5) species to the majority (7,5) species.

To interpret the full suite of anisotropy and TAS data, we propose the following mechanism for exciton transport within the coupled s-SWCNT thin films. The conclusion that diffusion-assisted exciton transport is hindered in majority species within polymer-free films may seem counterintuitive when considering the statistical probability of potential states to transfer to in going from bundle to bundle. However, it is important to note that the GSB peaks of majority species in polymer-free films are rapidly broadened and red-shifted (with respect to ground-state absorption) in the TA spectra. In contrast, GSB widths and energies of minority species in the same samples do not deviate significantly relative to the ground state. These observations imply strong electronic coupling between majority species in the polymer-free sample, which enables the exciton to efficiently locate the lowest energy states in the excited-state manifold of the majority species (likely due to states delocalized over multiple SWCNTs within a bundle), whereas excitons within minority species remain relatively localized on a single SWCNT. Statistically this makes sense, because majority species will be predominantly in contact with other majority species, whereas minority species will have a low probability of being in contact with other minority species within a bundle. This also implies that the energetic separation between the excited states of the majority and minority species is sufficient to minimize mixing of their excited state wavefunctions that would significantly alter the energy of the resulting excited state(s). GSB peaks in films containing residual polymer are not as broad or red-shifted as those for polymer-free films, suggesting that excitons in both majority and minority species are predominantly isolated on individual SWCNTs.

The impact of exciton delocalization on inter-bundle exciton transfer can be considered within the framework of electronic energy transfer,⁵¹ where the efficiency of exciton transfer is proportional to the spectral overlap between donor emission and acceptor absorption. We expect strong dipole overlap between donor and acceptor SWCNTs on adjacent bundles for films containing residual polymer due to the small bathochromic shifts for both majority and minority species, along with a fairly small PL Stokes shift (Fig. 3). Thus, diffusion-assisted exciton transfer between bundles appears to be efficient for both majority and minority species within these films.

Minority species in the polymer-free films may also undergo long-range energy transport even in the absence of wrapping polymer, as reflected by the similar $\tau(t)$ decay for minority species. However, exciton wave function delocalization in majority species within polymer-free films reduces the energy of the excited state, effectively 'trapping' the excitons into low-energy states which have poor energetic overlap and are weakly coupled to majority species acceptors in adjacent bundles. This mechanism would explain the negligible anisotropy decay of the majority species in both polymer-free films, and is consistent with the more rapid downhill energy transfer in polymer-free films. While the oscillator strength of the aggregate emission would be expected to decrease the electronic coupling between the donor and acceptor states, the broad red-shifted spectra of majority species now overlap better with the absorption of smaller bandgap minority species. Thus, one might still expect an enhancement of downhill exciton transfer to minority species both within a bundle and between bundles.

We conclude by considering the ultimate impact of polymer removal on exciton transport within a s-SWCNT device, i.e. diffusion to an exciton dissociation interface in a donor/acceptor photovoltaic device. On one hand, it is interesting to note that exciton diffusion still appears to be fairly efficient within the minority species. On the other hand, the rapid downhill energy transfer and hindered inter-bundle transport of majority species implies that a large fraction of excitons that are able to diffuse to exciton dissociation interfaces will have lost a significant fraction of the initial photon energy. This 'funneling' of most of the exciton population to minority species would likely lead to a loss of both voltage and photocurrent, the latter being related to the possible reduction in the charge transfer rate and yield for the minority species which have a lower thermodynamic driving force for interfacial exciton dissociation.⁵²

Conclusions

We circumvent the universal selectivity of a fluorene-based supramolecular polymer (SMP) for s-SWCNTs of any diameter by demonstrating an effective polymer exchange process that produces near-monochiral (6,5) and (7,5) samples dispersed using SMP. Replacement of the polymer modifies the strain exerted on s-SWCNTs by the wrapping polymer, which manifests as shifts in the optical excitonic transitions. Quantitative removal of the SMP results in thin film s-SWCNT networks where enhanced electronic coupling between neighbouring SWCNTs in a bundle results in a bathochromic shift and significant broadening of the first excitonic transition. Taken together, TA spectroscopy and anisotropy data suggest that this enhanced electronic coupling affords rapid downhill exciton energy transfer to the lowest energy s-SWCNT species, resulting in 'trapping' of the excitation on minority species within the same bundle (c.f., the lack of anisotropy decay). In contrast, while the wrapping polymer slows down the rate of downhill exciton energy transfer, the observed TA anisotropy suggests that excitons can move between s-SWCNTs in neighbouring bundles. These results highlight the complex

interplay between rapid downhill exciton energy transfer and long-range energy transport through a thin film network.

Conflicts of interest

There are no conflicts to declare.

Acknowledgements

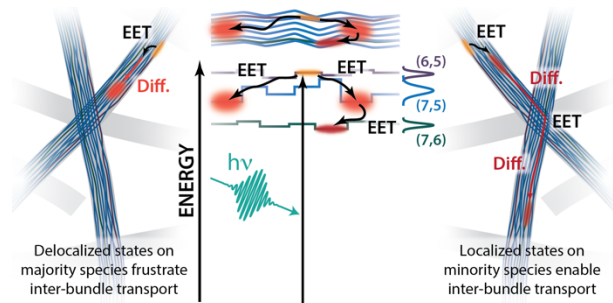
The authors acknowledge Dr. Zbyslaw Owczarczyk for synthesis and purification of the supramolecular polymer (SMP). This work was authored by the National Renewable Energy Laboratory, operated by Alliance for Sustainable Energy, LLC, for the U.S. Department of Energy (DOE) under Contract No. DE-AC36-08GO28308. Funding provided by the Solar Photochemistry Program of the Chemical Sciences, Geosciences, & Biosciences (CSGB) Division at the U.S. DOE Office of Science: Basic Energy Sciences. SMH acknowledges the U.S. DOE, Office of Science, Office of Workforce Development for Teachers and Scientists, Science Undergraduate Laboratory Internship (SULI) Program for funding her undergraduate internship. The views expressed in the article do not necessarily represent the views of the DOE or the U.S. Government.

Notes and references

1. M. S. Arnold, J. L. Blackburn, J. J. Crochet, S. K. Doorn, J. G. Duque, A. Mohite and H. Telg, *Phys. Chem. Chem. Phys.*, 2013, **15**, 14896.
2. D. J. Bindl and M. S. Arnold, *J. Phys. Chem. C*, 2013, **117**, 2390.
3. S. L. Guillot, K. S. Mistry, A. D. Avery, J. Richard, A.-M. Dowgiallo, P. F. Ndione, J. van de Lagemaat, M. O. Reese and J. L. Blackburn, *Nanoscale*, 2015, **7**, 6556.
4. J. L. Blackburn, *ACS Energy Lett.*, 2017, **2**, 1598.
5. A. D. Franklin, *Science*, 2015, **349**, aab2750.
6. G. J. Brady, A. J. Way, N. S. Safron, H. T. Evensen, P. Gopalan and M. S. Arnold, *Sci. Adv.*, 2016, **2**, e1601240.
7. A. Chortos, C. Zhu, J. Y. Oh, I. Pochorovski, J. W. F. To, N. Liu, U. Kraft, B. Murmann and Z. Bao, *ACS Nano*, 2017, **11**, 7925.
8. G. S. Tulevski, A. D. Franklin, D. Frank, J. M. Lobez, Q. Cao, H. Park, A. Afzali, S.-j. Han, J. B. Hannon and W. Haensch, *ACS Nano*, 2014, **8**, 8730.
9. M. L. Geier, J. J. McMorro, W. Xu, J. Zhu, C. H. Kim, T. J. Marks and M. C. Hersam, *Nature Nanotech.*, 2015, **10**, 944.
10. B. Kim, M. L. Geier, M. C. Hersam and A. Dodabalapur, *Sci. Rep.*, 2017, **7**, 39627.
11. W. A. Gaviria Rojas, J. J. McMorro, M. L. Geier, Q. Tang, C. H. Kim, T. J. Marks and M. C. Hersam, *Nano Lett.*, 2017, **17**, 4976.
12. B. A. MacLeod, N. J. Stanton, I. E. Gould, D. Wesenberg, R. Ihly, Z. R. Owczarczyk, K. E. Hurst, C. S. Fewox, C. N. Folmar, K. H. Hughes, B. L. Zink, J. L. Blackburn and A. J. Ferguson, *Energy Environ. Sci.*, 2017, **10**, 2168.
13. Y. Nonoguchi, A. Takata, C. Goto, T. Kitano and T. Kawai, *Sci. Technol. Adv. Mater.*, 2018, **19**, 581.
14. J. L. Blackburn, A. J. Ferguson, C. Cho and J. C. Grunlan, *Adv. Mater.*, 2018, **7**, 1704386.
15. J. Lefebvre, J. Ding, Z. Li, P. Finnie, G. Lopinski and P. R. L. Malenfant, *Acc. Chem. Res.*, 2017, **50**, 2479.

16. A. Szabó, C. Perri, A. Csató, G. Giordano, D. Vuono and J. B. Nagy, *Mater.*, 2010, **3**, 3092.
17. A. Nish, J.-Y. Hwang, J. Doig and R. J. Nicholas, *Nature Nanotech.*, 2007, **2**, 640.
18. K. S. Mistry, B. A. Larsen and J. L. Blackburn, *ACS Nano*, 2013, **7**, 2231.
19. S. K. Samanta, M. Fritsch, U. Scherf, W. Gomulya, S. Z. Bisri and M. A. Loi, *Acc. Chem. Res.*, 2014, **47**, 2446.
20. H. Wang and Z. Bao, *Nano Today*, 2015, **10**, 737.
21. G. J. Brady, Y. Joo, S. Singha Roy, P. Gopalan and M. S. Arnold, *Appl. Phys. Lett.*, 2014, **104**, 083107.
22. J. Ding, Z. Li, J. Lefebvre, F. Cheng, J. L. Dunford, P. R. L. Malenfant, J. Humes and J. Kroeger, *Nanoscale*, 2015, **7**, 15741.
23. G. Hills, C. Lau, A. Wright, S. Fuller, M. D. Bishop, T. Srimani, P. Kanhaiya, R. Ho, A. Amer, Y. Stein, D. Murphy, Arvind, A. Chandrakasan and M. M. Shulaker, *Nature*, 2019, **572**, 595.
24. B. Norton-Baker, R. Ihly, I. E. Gould, A. D. Avery, Z. R. Owczarczyk, A. J. Ferguson and J. L. Blackburn, *ACS Energy Lett.*, 2016, **1**, 1212.
25. T. Lei, I. Pochorovski and Z. Bao, *Acc. Chem. Res.*, 2017, **50**, 1096.
26. A. Chortos, I. Pochorovski, P. Lin, G. Pitner, X. Yan, T. Z. Gao, J. W. F. To, T. Lei, J. W. Will III, H. S. P. Wong and Z. Bao, *ACS Nano*, 2017, **11**, 5660.
27. R. D. Mehlenbacher, M.-Y. Wu, M. Grechko, J. E. Laaser, M. S. Arnold and M. T. Zanni, *Nano Lett.*, 2013, **13**, 1495.
28. R. D. Mehlenbacher, J. Wang, N. M. Kearns, M. J. Shea, J. T. Flach, T. J. McDonough, M.-Y. Wu, M. S. Arnold and M. T. Zanni, *J. Phys. Chem. Lett.*, 2016, **7**, 2024.
29. N. F. Hartmann, R. Pramanik, A.-M. Dowgiallo, R. Ihly, J. L. Blackburn and S. K. Doorn, *ACS Nano*, 2016, **10**, 11449.
30. Z. Zhang, Y. Che, R. A. Smaldone, M. Xu, B. R. Bunes, J. S. Moore and L. Zang, *J. Am. Chem. Soc.*, 2010, **132**, 14113.
31. Y. Joo, G. J. Brady, M. J. Shea, M. B. Oviedo, C. Kanimozhi, S. K. Schmitt, B. M. Wong, M. S. Arnold and P. Gopalan, *ACS Nano*, 2015, **9**, 10203.
32. T. Lei, X. Chen, G. Pitner, H. S. P. Wong and Z. Bao, *J. Am. Chem. Soc.*, 2016, **138**, 802.
33. Z. Li, J. Ding, C. Guo, J. Lefebvre and P. R. L. Malenfant, *Adv. Funct. Mater.*, 2018, **28**, 1705568.
34. F. Tshimitsu and N. Nakashima, *Nature Commun.*, 2014, **5**, 5041.
35. I. Pochorovski, H. Wang, J. I. Feldblyum, X. Zhang, A. L. Antaris and Z. Bao, *J. Am. Chem. Soc.*, 2015, **137**, 4328.
36. F. Tshimitsu and N. Nakashima, *Sci. Rep.*, 2015, **5**, 18066.
37. S. D. Stranks, C.-K. Yong, J. A. Alexander-Webber, C. Weisspfenning, M. B. Johnston, L. M. Herz and R. J. Nicholas, *ACS Nano*, 2012, **6**, 6058.
38. J. H. Choi and M. S. Strano, *Appl. Phys. Lett.*, 2007, **90**, 223114.
39. A. R. T. Nugraha, R. Saito, K. Sato, P. T. Araujo, A. Jorio and M. S. Dresselhaus, *Appl. Phys. Lett.*, 2010, **97**, 091905.
40. B. A. Larsen, P. Deria, J. M. Holt, I. N. Stanton, M. J. Heben, M. J. Therien and J. L. Blackburn, *J. Am. Chem. Soc.*, 2012, **134**, 12485.
41. L. Yang and J. Han, *Phys. Rev. Lett.*, 2000, **85**, 154.
42. T. K. Leeuw, D. A. Tsyboulski, P. N. Nikolaev, S. M. Bachilo, S. Arepalli and R. B. Weisman, *Nano Lett.*, 2008, **8**, 826.
43. J. Streit, C. R. Snyder, J. Campo, M. Zheng, J. R. Simpson, A. R. H. Walker and J. A. Fagan, *J. Phys. Chem. C*, 2018, **122**, 11577.
44. A. J. Ferguson, O. G. Reid, S. U. Nanayakkara, R. Ihly and J. L. Blackburn, *J. Phys. Chem. Lett.*, 2018, DOI: 10.1021/acs.jpclett.8b03074, 6864.
45. O. N. Torrens, D. E. Milkie, M. Zheng and J. M. Kikkawa, *Nano Lett.*, 2006, **6**, 2864.
46. T. Koyama, Y. Miyata, Y. Asada, H. Shinohara, H. Kataura and A. Nakamura, *J. Phys. Chem. Lett.*, 2010, **1**, 3243.
47. M. Grechko, Y. Ye, R. D. Mehlenbacher, T. J. McDonough, M.-Y. Wu, R. M. Jacobberger, M. S. Arnold and M. T. Zanni, *ACS Nano*, 2014, **8**, 5383.
48. R. D. Mehlenbacher, T. J. McDonough, N. M. Kearns, M. J. Shea, Y. Joo, P. Gopalan, M. S. Arnold and M. T. Zanni, *J. Phys. Chem. C*, 2016, **120**, 17069.
49. R. D. Mehlenbacher, T. J. McDonough, M. Grechko, M.-Y. Wu, M. S. Arnold and M. T. Zanni, *Nat. Commun.*, 2015, **6**, 6732.
50. C. J. Bardeen, *Annu. Rev. Phys. Chem.*, 2014, **65**, 127.
51. G. D. Scholes, *Annu. Rev. Phys. Chem.*, 2003, **54**, 57.
52. R. Ihly, K. S. Mistry, A. J. Ferguson, T. T. Clikeman, B. W. Larson, O. Reid, O. V. Boltalina, S. H. Strauss, G. Rumbles and J. L. Blackburn, *Nat. Chem.*, 2016, **8**, 603.

Table of Contents Entry - NR-ART-09-2019-007821



Exciton delocalization impacts complex interplay between rapid downhill exciton energy transfer and long-range energy transport through carbon nanotube networks.